obtained from successive Fourier difference maps coupled with isotropic least-squares refinement. Hydrogen atoms were modeled in idealized positions with fixed isotropic thermal parameters. Final Fourier difference maps exhibited no unusual features. A summary of crystal structure data is given in Table IV.

A New Family of Mesoporous Molecular Sieves Prepared with Liquid Crystal Templates

J. S. Beck,*[†] J. C. Vartuli,*[†] W. J. Roth,*[‡] M. E. Leonowicz,*[‡] C. T. Kresge,*[‡] K. D. Schmitt,[†] C. T-W. Chu,[‡] D. H. Olson,[†] E. W. Sheppard,[†] S. B. McCullen,[†] J. B. Higgins,[†] and J. L. Schlenker[†]

Contribution from the Mobil Research and Development Corporation, Central Research Laboratory, Princeton, New Jersey 08543, and Paulsboro Research Laboratory, Paulsboro, New Jersey 08066. Received June 30, 1992

Abstract: The synthesis, characterization, and proposed mechanism of formation of a new family of silicate/aluminosilicate mesoporous molecular sieves designated as M41S is described. MCM-41, one member of this family, exhibits a hexagonal arrangement of uniform mesopores whose dimensions may be engineered in the range of ~15 Å to greater than 100 Å. Other members of this family, including a material exhibiting cubic symmetry, have been synthesized. The larger pore M41S materials typically have surface areas above 700 m²/g and hydrocarbon sorption capacities of 0.7 cc/g and greater. A templating mechanism (liquid crystal templating—LCT) in which surfactant liquid crystal structures serve as organic templates is proposed for the formation of these materials. In support of this templating mechanism, it was demonstrated that the structure and pore dimensions of MCM-41 materials are intimately linked to the properties of the surfactant, including surfactant chain length and solution chemistry. The presence of variable pore size MCM-41, cubic material, and other phases indicates that M41S is an extensive family of materials.

Introduction

Two classes of materials that are used extensively as heterogenous catalysts and adsorption media are microporous (pore diameters ≤ ~20 Å) and mesoporous (~20–500 Å) inorganic solids.[1] The utility of these materials is manifested in their microstructures which allow molecules access to large internal surfaces and cavities that enhance catalytic activity and adsorptive capacity. A major subclass of the microporous materials is molecular sieves. These materials are exemplified by the large family of aluminosilicates known as zeolites in which the micropores are regular arrays of uniformly-sized channels.[2] Considerable synthetic effort has been devoted to developing frameworks with pore diameters within the mesoporous range, the largest synthesized to date being AlPO₄-8,[3] VPI-5,[4] and cloverite[5] which have pore diameters within the 8–13 Å range. Cacoxenite, a natural ferroaluminophosphate, has been structurally characterized as having ~14 Å channels that approach the mesoporous size range.[6] Mesoporous materials are typically amorphous or paracrystalline solids, such as silicas[7] or transitional aluminas[8] or modified layered materials such as pillared clays and silicates.[9–13] The pores in these materials are generally irregularly spaced and broadly distributed in size.[10] Despite these efforts, mesoporous molecular sieves with regular, well-defined channel systems have remained elusive.

Recently, a new family of mesoporous molecular sieves designated as M41S has been discovered.[14] MCM-41, one of the members of this extensive family of mesoporous sieves, possesses a hexagonal array of uniform mesopores. MCM-41 has been synthesized with uniform channels varying from approximately 15 Å to greater than 100 Å in size. The larger pore materials typically have surface areas above 700 m²/g and hydrocarbon

(1) IUPAC Manual of Symbols and Terminology, Appendix 2, Part 1, Colloid and Surface Chemistry, *Pure Appl. Chem.* **1972,** *31,* 578.

(2) See, for example: (a) Meier, W. M.; Olson, D. H. *Atlas of Zeolite Structure Types,* 3rd. ed. revised; Butterworth-Heineman & Co.: Guildford, 1992. (b) Szostak, R. *Molecular Sieves Principles of Synthesis and Identification;* Van Nostrand Reinhold: New York, 1989.

(3) Dessau, R. M.; Schlenker, J. L.; Higgins, J. B. *Zeolites* **1990,** *10,* 522–524.

(4) Davis, M. E.; Saldarriaga, C.; Montes, C.; Garces, J.; Crowder, C. *Nature* **1988,** *331,* 698–699.

(5) Estermann, M.; McCusker, L. B.; Baerlocher, C.; Merrouche, A.; Kessler, H. *Nature* **1991,** *352,* 320–323.

(6) Moore, P. B.; Shen, J. *Nature* **1983,** *306,* 356–358.

(7) Iler, R. K. *The Chemistry of Silica;* J. Wiley & Sons, Inc.: 1979.

(8) Wefers, K.; Misra, C. *Oxides and Hydroxides of Aluminum;* Alcoa Technical Paper No. 19, Revised, Alcoa Laboratories, 1987.

(9) Pinnavaia, T. J. *Science* **1983,** *220,* 365–371.

(10) (a) Vaughan, D. E. W.; Lussier, R. J. In *Proceedings of the 5th International Conference on Zeolites;* Rees, L. V. C., Ed.; Hyden, 1980; pp 94–100. (b) Meier, W. M. In *Studies in Surface Science & Catalysis;* Murakami, Y., Iijima, A., Ward, J. W., Eds.; Elsevier Science: 1986; Vol. 28, p 13.

(11) Vaughan, D. E. W. *ACS Symp. Ser.* **1988,** *368,* 308–325.

(12) (a) Landis, M. E.; Aufdembrink, B. A.; Chu, P.; Johnson, I. D.; Kirker, G. W.; Rubin, M. K. *J. Am. Chem. Soc.* **1991,** *113,* 3189–3190. (b) Yanagisawa, T.; Shimizu, T.; Kazuyuki, K.; Kato, C. *Bull. Chem. Soc. Japan* **1990,** *63,* 988–992.

(13) Tindwa, R. M.; Ellis, D. K.; Peng, G. Z.; Clearfield, A. *J. Chem. Soc., Faraday Trans. 1* **1985,** *81,* 545–548.

(14) Kresge, C. T.; Leonowicz, M. E.; Roth, W. J.; Vartuli, J. C.; Beck, J. S. *Nature* **1992,** *359,* 710–12.

[†] Mobil Research and Development Corporation, Central Research Laboratory.
[‡] Mobil Research and Development Corporation, Paulsboro Research Laboratory.

sorption capacities of 0.7 cc/g and greater. Other members of this family, including a cubic phase and other less well defined phases, have been identified.

A liquid crystal templating mechanism (LCT) in which surfactant liquid crystal structures serve as organic templates has been proposed for the formation of these materials.[14] Related mechanisms have been proposed for a number of systems in which inorganic structures of widely varying morphologies are deposited in the presence of preformed micellar arrays or micellar structures, as, for example, in the biochemical formation of bones and shells[15] from 40 different materials. However, in the biological system, the deposition of inorganic species is dynamically controlled, and products are dense structures whose ultimate morphology does not mimic the vesicle structures per se but mimics the biologically controlled "shape" of the vesicle array. Steigerwald[16] has used reverse micellar systems of Aerosol OT to form HgSe, CdSe, and CdTe particles. The proposed mechanism involved crystallization of the inorganic materials within the isolated micelles dispersed in hydrocarbon. Isolated micelles led to discrete particles.

Herein we describe the synthesis, physical properties, and proposed mechanism of formation of M41S materials.

Experimental Section

Materials. Silica sources were sodium silicate, N brand, 27.8% silica, P.Q. Corp.; HiSil, Pittsburgh Plate Glass; UltraSil, North American Silica Co.; tetramethylammonium silicate (0.5 TMA/SiO$_2$, 10% wt silica), SACHEM, Inc.; and tetraethyl orthosilicate, Aldrich. The quaternary ammonium surfactant compounds (C$_n$H$_{2n+1}$(CH$_3$)$_3$NX, X = Cl or Br) were obtained from Armak Chemicals, Kodak, Akzo Chemical, and American Tokyo Kasei. The C$_{16}$H$_{33}$(CH$_3$)$_3$NOH/Cl solution was prepared by batch exchange of a 29% by weight aqueous C$_{16}$H$_{33}$(CH$_3$)$_3$NCl solution with IRA-400(OH) exchange resin, Rohm and Haas. The effective exchange of hydroxide for chloride ion was ~30%. A C$_{12}$H$_{25}$(CH$_3$)$_3$NOH/Cl solution was prepared by batch exchange of a 50% by weight C$_{12}$H$_{25}$(CH$_3$)$_3$NCl solution (14% aqueous/36% isopropyl alcohol) in a similar matter. Sources of aluminum were sodium aluminate (technical grade), EM Science; aluminum sulfate, George Caine Chemical Company; and Catapal alumina, Condea. Trimethylsilyl chloride [(CH$_3$)$_3$SiCl] and hexamethyldisiloxane [((CH$_3$)$_3$Si)$_2$O] were obtained from Aldrich. Sulfuric acid (96.1%) was obtained from J. T. Baker Chemical Company. All chemicals were used as received.

Instrumentation. X-ray powder diffraction data were obtained on either a Scintag XDS 2000 diffractometer using Cu Kα radiation and an energy dispersive detector or on the X7A beamline at Brookhaven National Synchrotron Light Source. High resolution transmission electron microscopy (TEM) images and electron diffraction patterns were obtained on a JEOL 200 CX or a JEOL 2010 transmission electron microscope operated at 200 kV. Samples were examined either as microtomed sections or as grain mounts. Images from thin sections and thin grain edges were recorded under various focus conditions. Diffraction information from M41S materials is limited to relatively large d-spacings, and the diffracted intensities are much weaker than the unscattered beam. Images show contrast reversal upon going through Gaussian focus, as expected from the appearance of the electron diffraction pattern. Furthermore, no reversal in image contrast is observed at large underfocus conditions. These characteristics suggest that a weak phase object approximation is reasonable for the interpretation of these images. According to this interpretation, the light areas in the images correspond to a lack of scattering matter (pores), and the dark areas are concentrations of scattering material (walls). Scanning electron microscopy (SEM) was performed on a JEOL JXA-840 Scanning Electron Microscope using conventional sample preparation and imaging techniques.

Benzene sorption data were obtained on a computer-controlled 990/951 DuPont TGA system. The calcined sample was dehydrated by heating at 350 or 500 °C to constant weight in flowing He. Benzene sorption isotherms were measured at 25 °C by blending a benzene saturated He gas stream with a pure He gas stream in the proper proportions to obtain the desired benzene partial pressure. Argon physisorption measurements were conducted on a physisorption apparatus as previously described.[17] The method of Horváth and Kawazoe[18] was used to de-

Table I. Preparation of Surfactant Solutions

surfactant cation C$_n$H$_{2n+1}$(CH$_3$)$_3$N$^+$ n =	surfactant[a] (g)	water[b] (g)
8	11.60	34.80
9	12.25	36.75
10	12.89	38.67
12	14.18	42.54
14	15.47	46.43
16	16.77	50.23

[a] Each surfactant quantity represents 0.05 mol of surfactant; surfactant/silica mole ratio = 0.5. [b] Water was adjusted to make each surfactant 25 wt % in water.

termine the pore diameters of the products with pore diameters up to about 60 Å. In the pore regime above 60 Å in diameter, the Kelvin equation was applied.[19]

Temperature programmed amine desorption (TPAD) data were obtained on a DuPont series 9000/951 thermal analyzer under He with automatic titration of evolved base with sulfamic acid.[20]

Solid-state C-NMR spectra were obtained on a 200 MHz JEOL/Tecmag spectrometer, and solution C-NMR spectra were obtained either on a 360 MHz Chemagnetics NMR or a 60 MHz JEOL/Tecmag instrument. Si-NMR spectra were obtained in 9.5 mm zirconia rotors at 39.64 MHz spinning 4–4.2 KHz using 90° pulses at 1200-s intervals with high-power proton decoupling. Between 36 and 72 pulses (12–24 h) gave high quality spectra. Usually MAS Si-NMR of trimethylsilylated materials is obtained using cross polarization (CP) techniques to enhance sensitivity. CP is nonquantitative, and thus, single pulse excitation was used. Approximately 1200 s between pulses were needed for complete relaxation of the Q4 silicons of MCM-41. This is midway between the hours to days needed for dense phases such as quartz and the 1–5 min for zeolites. The Q4 relaxation time for MCM-41 is very similar to that of both amorphous silicas and crystalline SAPOs. Air was used as the drive gas to obtain as much benefit as possible from O$_2$ paramagnetic relaxation.[21] DSS (sodium 2,2-dimethyl-2-silapentane-5-sulfonate) and TMS (tetramethylsilane) were used as shift standards for solution and solid-state experiments, respectively.

Synthesis. Examples of typical preparations of the MCM-41 materials are listed below. The number in parentheses in the material designation, e.g. (40), indicates the X-ray powder diffraction d-spacing, of the calcined material, in angstroms (Å) of the first diffraction line (rounded to the nearest even Å unit). This nomenclature is used because MCM-41 materials can be prepared in a wide range of pore sizes, yet having essentially the same structure. We have rounded the d-spacing to the nearest even Å unit.

A. Synthesis of MCM-41(40) Using C$_{16}$H$_{33}$(CH$_3$)$_3$NOH/Cl. Two hundred grams of the C$_{16}$H$_{33}$(CH$_3$)$_3$NOH/Cl solution were combined with 2 g of Catapal alumina, 100 g of tetramethylammonium silicate solution, and 25 g of HiSil with stirring. This mixture was placed in a static autoclave at 150 °C for 48 h. After cooling to room temperature, the resulting solid product was recovered by filtration on a Buchner funnel, washed with water, and dried in air at ambient temperature. The X-ray diffraction pattern of the as-synthesized material exhibited a high intensity peak having a d-spacing of 43 Å and several lower angle peaks having d-spacings consistent with hexagonal indexing of hk0 reflections. The as-synthesized product was then calcined at 540 °C for 1 h in flowing nitrogen, followed by 6 h in flowing air. X-ray diffraction revealed a high intensity first peak having a d-spacing of 40 Å (representing a lattice contraction after calcination of about 3 Å) and several lower angle peaks having d-spacings with retention of the hexagonal hk0 indexing (Figure 1). The lattice contraction for MCM-41 materials varied depending on synthesis conditions. This calcined material is designated MCM-41(40). Found in the as-synthesized product (wt %): C, 35.4; N, 2.08; Al, 1.08; Si, 19.83; Ash (1000 °C), 46.9%. Found in the calcined product (wt %): C, <0.5; N, <0.09; Al, 2.59; Si, 39.85; Ash (1000 °C), 92.3%.

B. Synthesis of Siliceous MCM-41 (<40 Å). Forty grams of water, 18.7 g of N-brand (sodium silicate, 28.7% silica), and 1.2 g of sulfuric acid were combined with stirring. After allowing the resulting mixture to stir for 10 min, the appropriate surfactant (C$_n$H$_{2n+1}$(CH$_3$)$_3$NBr, n = 8, 9, 10, 12, 14, 16) template solution was added (see Table I), and the

(15) Heuer, A. H.; Fink, D. J.; Laraia, V. J.; Arias, J. L.; Calvert, P. D.; Kendall, K.; Messing, G. L.; Blackwell, J.; Rieke, P. C.; Thompson, D. H.; Wheeler, A. P.; Veis, A.; Caplan, A. I. *Science* **1992**, *255*, 1098–1105.
(16) Steigerwald, M. L. *J. Am. Chem. Soc.* **1988**, *110*, 3046–3050.
(17) Borghard, W. S.; Sheppard, E. W.; Schoennagel, H. J. *Rev. Sci. Instrum.* **1991**, *62*, 2801–2809.
(18) Horváth, G.; Kawazoe, K. *J. Chem. Eng. Jpn.* **1983**, *16*, 470–475.

(19) Gregg, S. J.; Sing, K. S. W. *Adsorption, Surface Area, and Porosity*, 2nd ed.; Academic Press, Inc.: 1982.
(20) Kerr, G. T.; Chester, A. W. *Thermochim. Acta* **1971**, *3*, 113–124.
(21) (a) Cookson, D. J.; Smith, B. E. *J. Magn. Reson.* **1985**, *63*, 217–218. (b) Klinowski, J.; Carpenter, T. A.; Thomas, J. M. *J. Chem. Soc., Chem. Commun.* **1986**, 956–958.

10836 *J. Am. Chem. Soc., Vol. 114, No. 27, 1992*

Beck et al.

Table II. Amount of Mesitylene (MES) Added To Synthesize the Desired Pore Size MCM-41 as Determined by Argon Physisorption

Ar pore size	40	45	50	65
amt of MES added (g)	0	6	9	22

resulting gel was allowed to stir for 0.5 h. (In order to make a direct comparison between surfactants, each reaction was carried out at equivalent surfactant/silica mole ratio (0.5) and each surfactant was added as a 25 wt % aqueous solution.) Twenty grams of water were then added to the gel. The gels were heated at 100 °C for 144 h. The resulting solid products were recovered and processed to a calcined form using the method described above.

C. **Synthesis of Aluminosilicate MCM-41 (<40 Å). For the $C_{12}H_{25}(CH_3)_3N^+$ Directed Preparation.** Sodium aluminate (8.3 g) was added slowly to a solution containing 184 g of a $C_{12}H_{25}(CH_3)_3NOH/Cl$ solution diluted with 480 g of water. Fifty grams of Ultrasil silica, 200 g of a tetramethylammonium silicate solution, and 26.4 g of a tetramethylammonium hydroxide solution (25 wt %) were then added with stirring. This combined mixture was then loaded into an autoclave and heated with stirring at 100 °C for 24 h. The resulting solid product was recovered and processed to a calcined form using the method described above.

For the $C_{14}H_{29}(CH_3)_3N^+$ Directed Preparation. Sodium aluminate (4.2 g) was added slowly to a solution containing 16 g of $C_{14}H_{29}$-$(CH_3)_3NBR$ in 100 g of water. One hundred grams of tetramethylammonium silicate solution, 25 g of HiSil silica, and 14.2 g of a tetramethylammonium hydroxide solution (25 wt %) were then added with stirring. This combined mixture was then loaded into an autoclave and heated with stirring at 100 °C for 24 h. The resulting solid product was recovered and processed to a calcined form using the method described above.

For the $C_{16}H_{33}(CH_3)_3N^+$ Directed Preparation. Two hundred grams of the $C_{16}H_{33}(CH_3)_3NOH/Cl$ solution were combined with 4.2 g of sodium aluminate, 100 g of a tetramethylammonium silicate solution, and 25 g of HiSil. This mixture was placed in an autoclave with stirring at 120 °C for 24 h. The resulting solid products were recovered and processed to a calcined form as described above.

D. **Synthesis of MCM-41 Materials (>40 Å) Prepared with the Auxiliary Organic Mesitylene.** Eighty grams of the $C_{16}H_{33}$-$(CH_3)_3NOH/Cl$ were combined with 1.65 g of sodium aluminate. Forty grams of a tetramethylammonium silicate solution and 10 g of HiSil were then added. While the gel was stirred at room temperature, the auxiliary organic mesitylene (MES) was added as the last ingredient (the quantity of MES added ranged from 0–22 g, corresponding to a MES/SiO₂ mole ratio of 0–2.5). See Table II for the amount of MES added to produce the desired pore size MCM-41. The gel was then loaded into an autoclave and heated to 105 °C with stirring. After 4 h of heating, the reaction was quenched with cold water, and the contents were removed. The resulting solid products were recovered and processed to a calcined form as described above.

Trimethylsilylation of MCM-41. In a typical experiment, 0.50 g of MCM-41(40), 10 g (CH₃)₃SiCl (TMSCl), and 15 g of ((CH₃)₃Si)₂O (HMDS) were refluxed overnight with magnetic stirring under N₂. The volatiles were stripped on a rotary evaporator, and the dry powder was washed 2 or 3 times with 10 mL of reagent grade acetone with centrifuging. Material recovery was typically >98%.

Results

The M41S materials described herein may be synthesized from a variety of silica sources and can be prepared in either silicate or aluminosilicate forms. As illustrated in the examples above, these materials may be prepared over a broad time/temperature regime. The as-synthesized M41S products are easily isolated from hydrothermal syntheses by filtration and water washing. These materials typically contain large amounts of surfactant after thorough water washing. Carbon to nitrogen atomic ratios of the as-synthesized materials are consistent with the surfactant remaining intact throughout the synthesis. This observation will be discussed further in the NMR results. The final silicate and aluminosilicate, mesoporous materials are obtained by calcination in N₂ and air. The nature of the surfactant, including its carbon chain length, aqueous concentration, the surfactant/silicon mole ratio, and reaction conditions are all critical factors in determining the nature of the product.

Characterization data for the M41S family of mesoporous molecular sieves are discussed below. MCM-41 has been the species most investigated. We propose a synthesis mechanism that
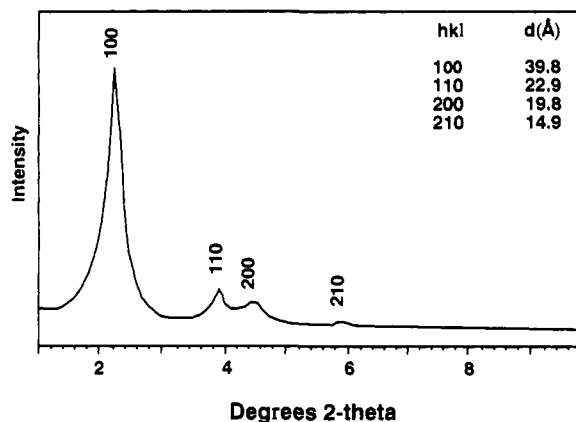
Figure 1. Powder X-ray diffraction pattern of calcined MCM-41(40).

hkl	d(Å)
100	39.8
110	22.9
200	19.8
210	14.9

is consistent with the characterization data.

Characteristics of Hexagonal Phase MCM-41. The transmission electron micrographs in Figure 2 show the regular, hexagonal array of uniform channels for various MCM-41(n) materials with pore sizes from 20 to about 100 Å. The number in parentheses in the material designation, e.g. (40), indicates the X-ray powder diffraction d-spacing, of the calcined material, in angstroms (Å), of the first diffraction line rounded to the nearest even Å unit. The transmission electron micrograph of preparation A, described above, is represented in Figure 2b. The MCM-41 preparations with pore sizes greater than 40 Å were synthesized using reaction mixtures with added auxiliary organics (see below). The hexagonal structure, with each pore surrounded by six neighbors, is present in all samples. The most regular hexagonal arrangement of uniform pores is usually observed for the smaller pore size materials (<40 Å), which were produced in the absence of any auxiliary organic, with regularity decreasing as the pore size increases.

Synchrotron X-ray powder diffraction data for a sample of MCM-41(40) are shown in Figure 1. The observation of 3–5 peaks which can be indexed on a hexagonal lattice is typical of MCM-41 materials.

The BET surface area of the MCM-41(40) (preparation A) was 1040 m²/g with exceptionally high sorption capacities (by weight, 49% n-hexane at 40 Torr (at 21 °C) and 67% benzene at 50 Torr (at 25 °C)). Figure 3 shows the benzene sorption isotherm of this material, along with an isotherm for zeolite Y, and of an amorphous silica for comparison. The isotherm for the mesoporous molecular sieve exhibits a sharp inflection characteristic of capillary condensation within uniform pores, where the p/p_0 position of the inflection point is related to the diameter of the pore.[18,19] Argon physisorption data both confirm the uniformity and indicate the pore size (~40 Å) of this MCM-41(40) sample. Figure 4 illustrates the Horváth–Kawazoe plot of the argon physisorption for the MCM-41(40) sample indicating a narrow pore size distribution (width at half height = 4 Å) similar to those of molecular sieves and unlike those of amorphous materials.

Surfactant Chain Length Variation in the Synthesis of MCM-41. When quaternary ammonium surfactants ($C_nH_{2n+1}(CH_3)_3N^+$) with different alkyl chain lengths (n = 8, 9, 10, 12, 14, 16) were used, MCM-41 materials exhibiting different XRD spacings were obtained. The effect of surfactant chain length on MCM-41 products on both the location of the first X-ray diffraction lines (d_{100}) of the calcined products (siliceous and aluminosilicate) and approximate pore size as determined by argon physisorption is illustrated in Table III. The approximate pore size calculated by argon physisorption should be less than the repeat distance (a_0) as determined by X-ray diffraction (hexagonal $a_0 = 2d_{100}/\sqrt{3}$) because the repeat distance includes the pore wall. This difference between these two determinations gives an indication of the pore wall thickness. Variations in this wall thickness depending on the surfactant chain length system may be a result of the synthetic conditions. However, these variations are most likely due to the
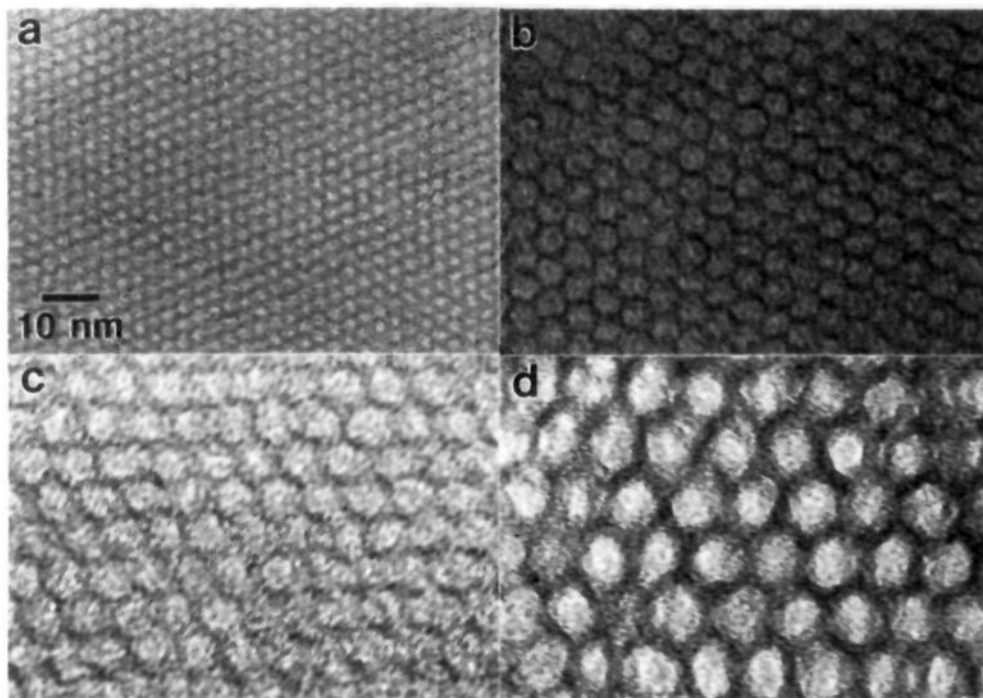
Figure 2. Transmission electron micrographs of several MCM-41 materials having Ar pore sizes of (a) 20, (b) 40, (c) 65, and (d) 100 Å.
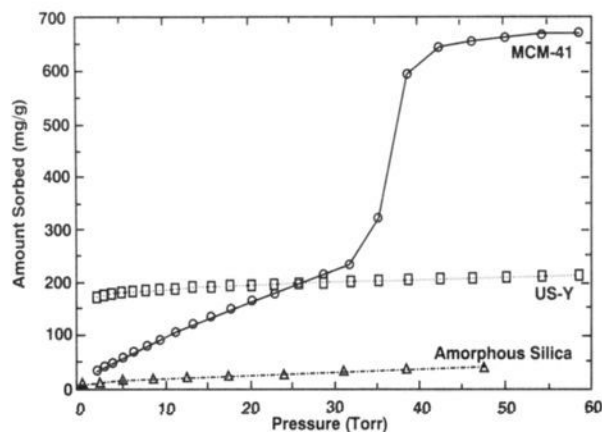

Figure 3. Benzene adsorption isotherms of MCM-41(40), zeolite Y, and amorphous silica at 25 °C.

Table III. Effect of Surfactant Chain Length on MCM-41 Pore Size, XRD d_{100} Peak Location, Hexagonal Unit Cell Parameter, a_0, and Benzene Uptake

surfactant chain length $C_nH_{2n+1}(CH_3)_3N^+$ $n =$	XRD d_{100} d-spacing (Å)	$a_0{}^a$ (Å)	Ar pore size (Å)	total benzene uptake (wt %) at 50 Torr
Siliceous Products				
8	27	31	18	16
9	28	32	21	37
10	29	33	22	32
12	29	33	22	36
14	33	38	30	54
16	35	40	37	64
Aluminosilicate Products				
12	31	36	–	43
14	34	39	34	40
16	39	45	38	61

$^a a_0 = 2d_{100}/\sqrt{3}$.

precision of the pore size calculation. Nevertheless, the data indicate that MCM-41 pore diameter generally increases with surfactant chain length under comparable reaction conditions. This suggestion is supported by the benzene sorption data of the siliceous products (Figure 5) which generally show a shift in the capillary condensation point to higher benzene partial pressure for materials prepared with increasing surfactant chain length. This shift is indicative of the filling of larger pores. Furthermore, the total benzene uptake was generally found to increase with surfactant chain length.

Addition of Auxiliary Organics to MCM-41 Synthesis Mixtures. The typical MCM-41 reaction mixture was also modified by the addition of an auxiliary organic, mesitylene (MES) (synthesis D). The molar ratio of MES to $C_{16}H_{33}(CH_3)_3N^+$ in this study ranged from 0 to 2.5. Incremental addition of MES resulted in a proportional increase in d-spacing of the X-ray d_{100} peak. This increase was accompanied by retention of the hexagonal relationship with the X-ray diffraction pattern of each material exhibiting 3–4 peaks related by hexagonal symmetry. As shown in Figure 6, a plot of MES/$C_{16}H_{33}(CH_3)_3N^+$ mole ratio versus both d_{100} and pore size, as determined by argon physisorption, results in a linear correlation within this range of reactant ratios. Figure 2c is a transmission electron micrograph of the material

prepared with a MES/$C_{16}H_{33}(CH_3)_3N^+$ ratio of 2.0. (See Table II for synthetic data.)

Figure 7 shows the benzene sorption isotherms for the several materials prepared with the auxiliary organic. All show the large sorption capacity characteristic of MCM-41. The isotherms show a gradual shift in capillary condensation to higher benzene pressure with increasing mesitylene content. The material formed with the highest MES/$C_{16}H_{33}(CH_3)_3N^+$ ratio, 1.5, shows only the very beginnings of capillary condensation at the highest benzene pressure examined (60 Torr, $p/p_0 = 0.6$). However, argon isotherms clearly show capillary condensation for these larger pore size materials. Both pore size and pore volume increase with increasing d_{100}.

Larger pore materials were prepared from modified reaction mixtures having MES/$C_{16}H_{33}(CH_3)_3N^+$ ratios greater than 3. Additional water and longer reaction times were used in these preparations. The products display X-ray powder diffraction patterns exhibiting a single broad line in the extreme low angle region ($2\theta < 1°$) or sometimes only enhanced intensity in the extreme low angle region because our instruments cannot measure reliably diffraction below 1° 2θ. However, TEM examination shows that these materials are MCM-41 with a range of d_{100}
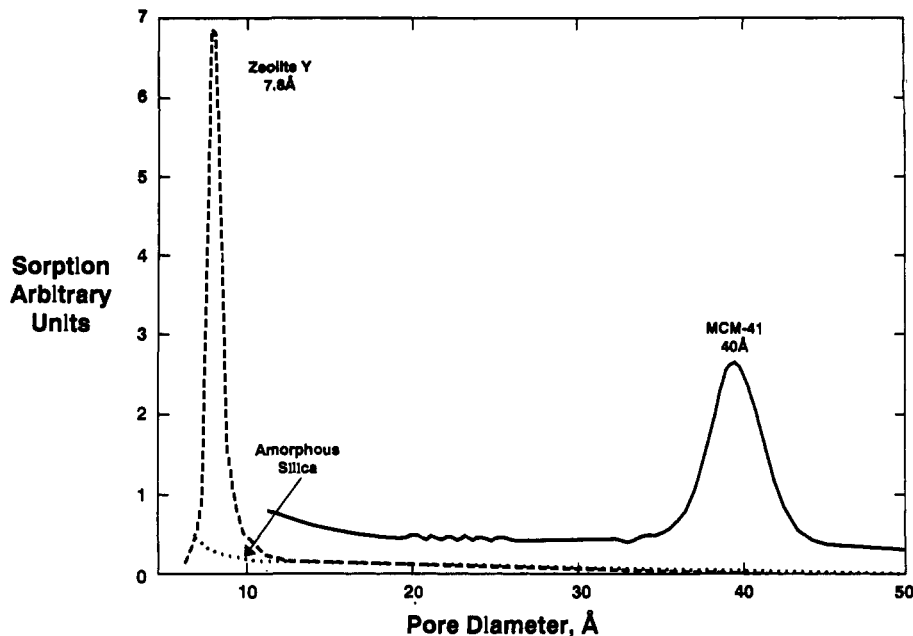
Figure 4. Horváth-Kawazoe pore size distributions for MCM-41(40), zeolite Y, and amorphous silica.
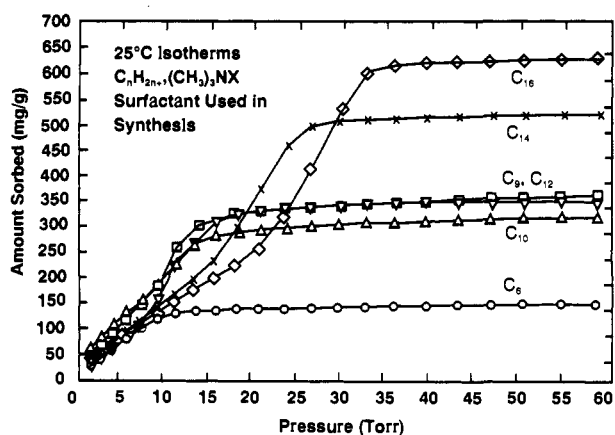

Figure 5. Benzene adsorption isotherms for siliceous MCM-41 materials prepared with varying surfactant chain length (n = 8, 9, 10, 12, 14, and 16. X = Br).
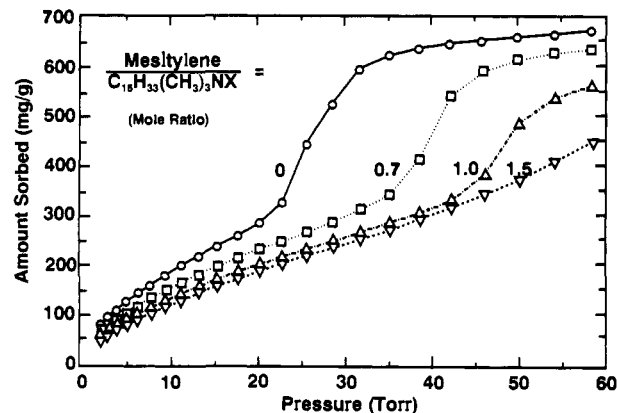

Figure 7. Benzene adsorption isotherms of MCM-41 materials prepared with addition of mesitylene auxiliary organic (X = OH/Cl).
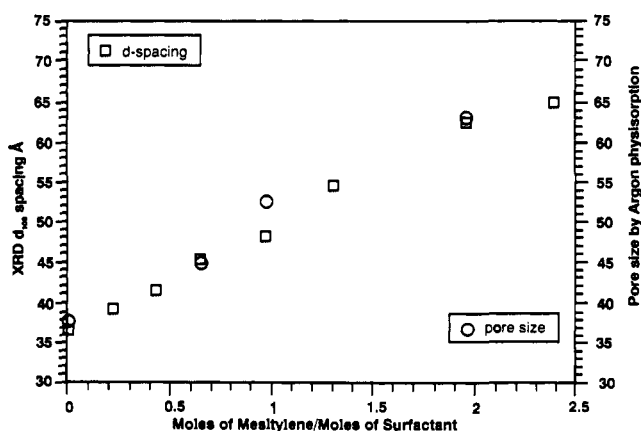

Figure 6. Powder X-ray diffraction d_{100} spacing and Horváth-Kawazoe pore size as a function of mesitylene/surfactant molar ratio.

Figure 8. Thermal gravimetric analysis (solid) and temperature programmed amine desorption (dashed) of an as-synthesized MCM-41(40) made using $C_{16}H_{33}(CH_3)_3N^+$ and containing 2.8% Al. The heating rate was 20 °C/min.

between 85 and 120 Å (for example, Figure 2d illustrates a material with ca. 100 Å pores). These materials display somewhat irregular, yet essentially hexagonal, pore arrangements. In agreement with these results, argon physisorption derivative uptake curves are significantly broader for these larger pore materials indicating a wider pore size distribution. It is, thus, apparent that MCM-41(nÅ) materials comprise an extensive family having
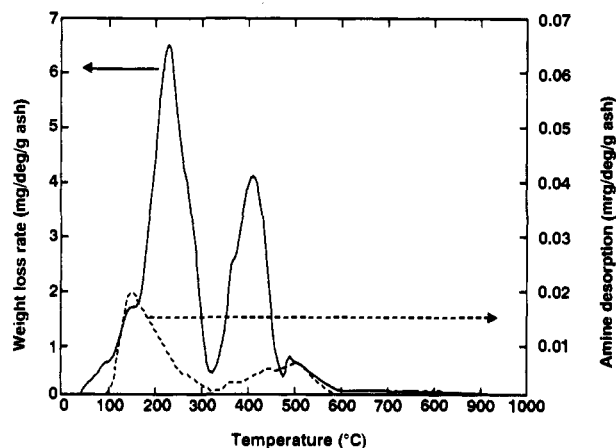
uniform, controllable sized mesopores.

Thermogravimetric Analysis. Temperature programmed amine desorption analysis, TPAD, of as-synthesized aluminum containing MCM-41(40) was carried out from room temperature to 900 °C under flowing He with titration of the evolved base.[20] The differential weight loss and base evolution curves are shown as Figure
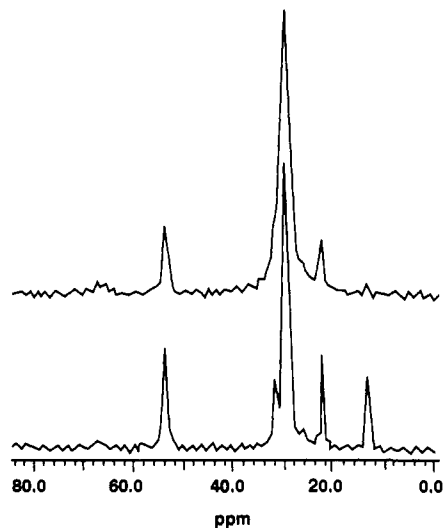
Figure 9. Single pulse (lower) and cross polarization (upper) 50.18 MHz magic angle spinning, H-1 decoupled, C-NMR spectra of an MCM-41-(40) synthesized with $C_{16}H_{33}(CH_3)_3N^+$. The spectral width was 10 kHz, the spinning rate was 4.25 kHz, and the decoupler field 50 kHz. The cross polarization spectrum was obtained using 432 1-ms single contacts at 1-s intervals. The single pulse spectrum was obtained using 888 90-deg pulses at 3-s intervals with gated high power decoupling.

8. At least two peaks are observed in these scans. The maxima for weight loss and $(CH_3)_3N$ evolution do not exactly correspond suggesting decomposition and desorption are not simultaneous. If the weight loss maxima are assigned to "low"-temperature and "high"-temperature changes, the molecular weight of the decomposing species is calculated to be 312 g/mol for the low-temperature and 339 g/mol for the high-temperature species. This is reasonably close to the sum of the molecular weights (283 g/mol) expected for decomposition of $C_{16}H_{33}(CH_3)_3N^+$ to hexadecene (224 g/mol) and trimethylamine (59 g/mol).

The bimodal amine desorption probably results from the association of $C_{16}H_{33}(CH_3)_3N^+$ with siloxy groups and Brønsted sites, the latter from the aluminum. The siloxy groups are stronger bases (silanols are weaker acids) and should promote Hoffmann elimination at lower temperature. If this is the case, the low-temperature peak corresponds to about 14% of the silicons being silanols, similar to the 14.6% found after calcination by trimethylsilylation (see below). The high-temperature peak, if associated with aluminum, would correspond to 2.8% Al, which is in excellent agreement with the 2.9% Al reported in the elemental analysis of the sample.

NMR Studies of MCM-41. Solid-state C-NMR spectra of several as-synthesized MCM-41 materials were obtained. Intact $C_{16}H_{33}(CH_3)_3N^+$ was identified by comparison of the peaks obtained with those found for $C_{16}H_{33}(CH_3)_3N^+$ in solution. Typical spectra are shown in Figure 9. The spectra are striking for the sharpness of the peaks. The organic cross-polarizes very poorly, and normal, single pulse experiments give very good spectra. The hydrocarbon ends of the $C_{16}H_{33}(CH_3)_3N^+$ are so mobile that they show essentially no intensity in the CP spectra. The sharpness of the peaks alone might be due to ordering in the solid, but the cross-polarization behavior is more likely the result of molecular mobility of the type associated with surfactants in micellar arrays. The fact that the polar ends of the surfactant molecules can be cross polarized shows that the surfactant is not present as a "solution" species, again consistent with the presence of a micellar array.

Si-NMR spectra of MCM-41 closely resemble those of amorphous silica[22] suggesting a broad range of Si–O–Si (T–O–T) bond angles in this material. In both cases the spectra can be separated into three very broad peaks (MCM-41: −92.4, −101.7, −110.5; amorphous silica: −90.6, −99.8, −109.3) by appropriate
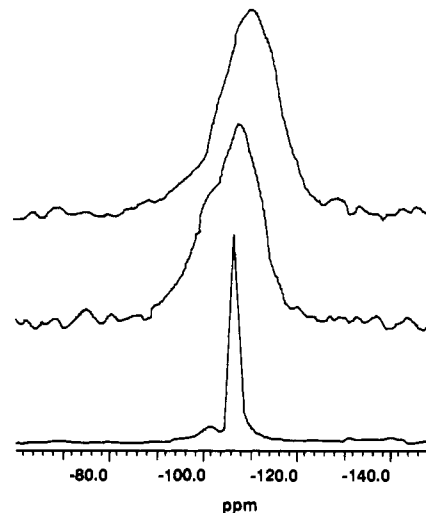

Figure 10. Comparative 71.53 MHz magic angle spinning Si-NMR spectra of siliceous samples of amorphous silica (upper), MCM-41(40) (middle), and zeolite-Y (lower). Samples were calcined at 500 °C under flowing N_2 before obtaining the spectra which were obtained spinning at 5.000 kHz, using 90-deg pulses at 300-s intervals.

choice of CP conditions. Figure 10 illustrates the Si-NMR of siliceous MCM-41, amorphous silica, and zeolite Y for comparison. Quantitative analysis was not possible since the peaks were broad and overlapping and could only be resolved using nonquantitative CP techniques. However, deconvolution of the CP–MAS Si-NMR of calcined and uncalcined MCM-41 suggested about 20 ± 10% and 40 ± 20% of the silicon atoms, respectively, were silanols (Q_3), similar to the results for amorphous silicas before and after heating to 500 °C.[23]

Trimethylsilylation of MCM-41. Silanol silylation via reaction with chlorotrimethylsilane has been reported for a number of silanol containing materials including amorphous silica,[24] kenyaite, and magadiite.[25,26] For amorphous silica, 20–40% of the silicon atoms are silanols, but only about 9% of the silicon atoms (50–25% of the silanols) appear to be accessible for silylation. For kenyaite and magadiite all of the 16–20% silanols can be derivatized (the silanol peaks are well resolved in these materials so the initial silanol concentration can be determined from Si-NMR on the untreated material). Silicon atoms in a trimethylsilyl (TMS) moiety show peaks at ~12 ppm in the Si-NMR. After trimethylsilylation a Q_3 silanol is converted to a silicon atom surrounded by four other silicons (Q4), and thus takes on the typical shift of −100 to −120 ppm and often is indistinguishable from Q_4 silicon atoms. In terms of stoichiometry, the TMS silicon atom concentration is equal to the original silanol concentration, so its peak area relative to the total of Q4 silicons after derivatization is the percent of silanol silicon atoms or at least the percent converted.

There is reasonable agreement between the concentration of silanols found in the trimethylsilylated material, as determined by Si-NMR, and the amount of $C_{16}H_{33}(CH_3)_3N^+$ from TPAD. This suggests the silanols may be present primarily as charge balancing siloxy similar to the silanols in ZSM-5 at $Si/Al_2 > 40$ (with tetrapropylammonium bromide as template[27]).

(22) Maciel, G. E.; Sindorf, D. W. *J. Am. Chem. Soc.* **1980**, *102*, 7606–7607.

(23) Sindorf, D. W.; Maciel, G. E. *J. Am. Chem. Soc.* **1983**, *105*, 1487–1493.

(24) (a) Sindorf, D. W.; Maciel, G. E. *J. Phys. Chem.* **1982**, *86*, 5208–5214. (b) Sindorf, D. W.; Maciel, G. E. *J. Phys. Chem.* **1983**, *87*, 5516–5521. (c) Sindorf, D. W.; Maciel, G. E. *J. Am. Chem. Soc.* **1983**, *105*, 3767–3776.

(25) (a) Yanagisawa, T.; Kuroda, K.; Kato, C. *Reactivity Solids* **1988**, *5*, 167–175. (b) Yanagisawa, T.; Kuroda, K.; Kato, C. *Bull. Chem. Soc. Jpn.* **1989**, *61*, 3743–3745.

(26) (a) Rojo, J. M.; Sanz, J.; Ruiz-Hitzy, E.; Serratosa, J. M. *Z. Anorg. Allg. Chem.* **1986**, *540/541*, 227–233. (b) Ruiz-Hitzky, E.; Rojo, J. M. *Nature* **1980**, *287*, 28–30.

(27) Dessau, R. M.; Schmitt, K. D.; Kerr, G. T.; Woolery, G. L.; Alemany, L. B. *J. Catal.* **1987**, *104*, 484–486.
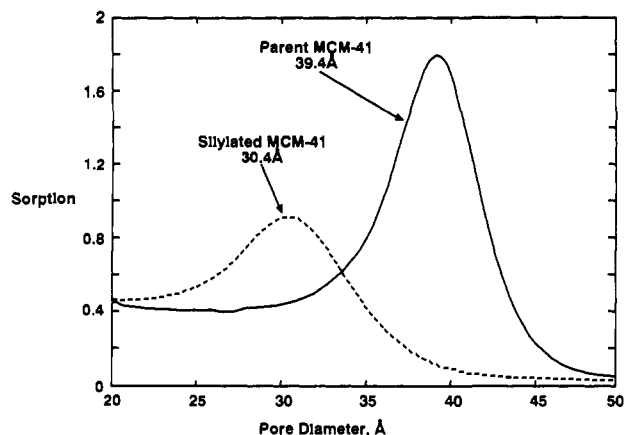
10840 *J. Am. Chem. Soc., Vol. 114, No. 27, 1992*

Beck et al.

Figure 11. Horváth-Kawazoe pore size distribution for MCM-41(40) and silylated version.

Table IV. Comparison of Experimental MCM-41 Relative X-ray Intensities with Calculated Intensities for Framework and Cylindrical Shell Wall Models

hkl	exptl MCM-41 data	framework wall model[a]	cylindrical shell model
100	100	100	100
110	1.8	11	2
200	1.6	10	4
210	0.2	7	1
300	b	1	<1
220	b	1	<1
310	b	2	<1

[a] 81 (7) is chosen because its a_0 cell parameter is closest to that obtained from the MCM-41(40) preparation.[28] [b] Not observed.

Figure 11 shows the Horváth–Kawazoe transformed argon physisorption results on the trimethylsilylated TMS-MCM-41 and its calcined parent. The pore diameter decreases from 39.4 to 30.4 Å upon conversion of the silanols to TMS groups. The 4.5 Å decrease in radius is consistent with that predicted for replacement of each silanol proton by a TMS group based on CPK models.[28]

Diffraction Studies of MCM-41. The exact structural nature of the silicate/aluminosilicate framework in the pore walls of these materials is uncertain. The presence of distinct *hk*0 reflections in the X-ray diffraction data suggests a framework with long range regularity. The *hk*0 reflections can be indexed on a hexagonal lattice, but the observation of only *hk*0 reflections in the experimental diffraction data (Figure 1) is unusual for material ordered in three dimensions.

It is obvious from the TEM data (Figure 2b) that concentrations of scattering matter occur at about 40 Å intervals along [100] in MCM-41(40) (preparation A). X-ray powder patterns were calculated from several models for comparison with the experimental data. We first considered zeolite framework models based on the 81(n) series[29] and on a series related to the NNFF models proposed by Barrer and Villager.[30] Both these models are based on a hexagonal three-dimensional tetrahedral framework. At the opposite extreme, diffraction data from a pore model wherein the walls contained a continuous distribution of scattering matter were calculated for a hexagonal array of cylindrical shells based on equations derived by Oster and Riley.[31] The results of two of these calculations were compared with experimental MCM-41 X-ray data as illustrated in Table IV.

An interesting result of these model calculations is the qualitative similarity in the diffraction intensities from different models. Both models exhibit strong 100 reflections and several low-order weak *hk*0 reflections (Table IV). All higher order *hk*0 and *hkl*

reflections (the cylindrical shell model has only *hk*0 reflections) have calculated relative intensities less than 1% of the strong 100 reflections. Based on these results, as well as additional model studies and theoretical calculations, we conclude that diffraction intensities from any model with a hexagonal array of large cylindrical pores with relatively thin pore walls will exhibit a similar pattern. Thus, for these materials, diffraction intensities are of limited use in determining the structural nature of the pore walls.

Additional insight into the nature of the pore walls may be obtained from the ^{29}Si-NMR data. The very broad MAS ^{29}Si-NMR resonance (Figure 10) indicates a broad range of T–O–T angles in the pore walls[32] as indicated above. This is consistent with a framework that lacks precise repeats of Si positions at the second nearest neighbor (T–T) length scale.

Microscopy. Microscopy reveals that the particle morphology of MCM-41 materials is variable, but it is possible to obtain discrete hexagonally shaped particles. (These materials were prepared with the dodecyltrimethylammonium cation.) Figure 12 (parts a and b) illustrate smaller particles with distinct hexagonal morphology (0.05–0.2 μm) which were imaged at higher magnifications. These smaller hexagonal particles were relatively easy to find, although they did not constitute the majority of particles observed in this size range. In each of these images, hexagonal arrays of micropores are evident, and rows of pores are parallel to the hexagonal particle edges. In one such preparation, these particles are large enough, over 2 μm in diameter, for the hexagonal morphology to be easily observed in the SEM (Figure 12c). These large hexagonal particles exhibit a range of surface textures from smooth through pitted. Although these large particles are too thick for electron beam penetration in the TEM, we have observed fringes and pore structure around thin edges (Figure 12d). Large areas of hexagonal pore packing are easily imaged in thin areas of these particles.

(28) CPK is a registered trademark of Harvard Apparatus, Inc.
(29) Smith, J. V.; Dytrych, W. J. *Nature* **1984**, *309*, 607–608.
(30) Barrer, R. M.; Villager, H. *Z. Kristallogr.* **1969**, *128*, 352–370.
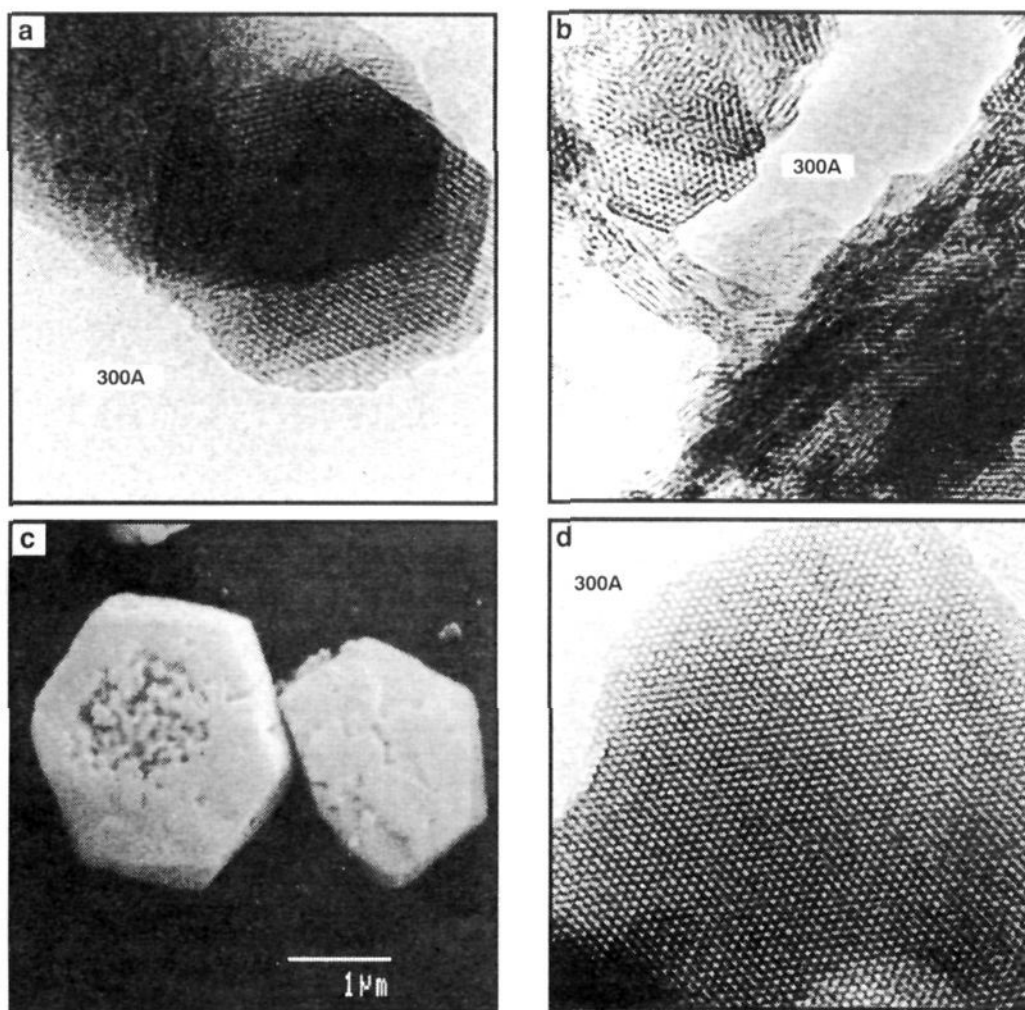(31) Oster, G.; Riley, D. P. *Acta Crystallogr.* **1952**, *5*, 272–276.

(32) (a) Tossell, J. A. *Phys. Chem. Minerals* **1984**, 137–141. (b) Magi, M.; Lippmaa, E.; Samoson, A.; Engelhardt, G.; Grimmer, A.-R. *J. Phys. Chem.* **1984**, *88*, 1518–1522. (c) Newsam, J. M. *J. Phys. Chem.* **1987**, *91*, 1259–1262. (d) James, N.; Oldfield, E. *J. Am. Chem. Soc.* **1985**, *107*, 6769–6775. (e) Sherriff, B. L.; Grundy, H. D. *Nature* **1988**, *332*, 819–821.
(33) Harris, R. K.; Knight, C. T. G. *J. Mol. Struct.* **1982**, *78*, 273–278.
(34) See, for example: (a) Luzzati, V. In *Biological Membranes*; Chapman, D., Ed.; Academic Press, Inc.: 1968; p 71. (b) Ekwall, P. In *Advances in Liquid Crystals*; Brown, G. H., Ed.; Academic Press, Inc.: 1971; p 1. (c) Ekwall, P.; Mandell, L.; Fontell, K. In *Liquid Crystals*; Brown, G. H., Ed.; Gordon and Breach Ltd.: 1969; p 325. (d) Winsor, P. A. *Chem. Rev.* **1968**, *68*, 1–40.
(35) Chang, C. D.; Bell, A. T. *Catal. Lett.* **1991**, *8*, 305–316.
(36) (a) Kerr, G. T. *J. Phys. Chem.* **1966**, *70*, 1047–1050. (b) Circ, J. J. *Colloid Interfac. Sci.* **1968**, *28*, 315–324. (c) Ueda, S.; Koizumi, M. *Am. Mineral.* **1979**, *64*, 172–179. (d) Guth, J. L.; Caullet, P.; Jacques, P.; Wey, R. *Bull. Soc. Chim.* **1980**, *3–4* (part 1), 121–126. (e) Ueda, S.; Kageyama, N.; Koiszumi, M. In *International Conference on Zeolites, 6th, Reno*; Olson, D. H., Bisio, A., Eds.; Guilford: Amsterdam, 1984; pp 905–924, and references therein. (f) Davis, M. E.; Lobo, R. F. *Chem. Mater.* **1992**, *4*, 756–768.
(37) Barrer, R. M. In *ACS Symposium Series 398, Zeolite Synthesis*; Occelli, M. L., Robson, H. E., Eds.; American Chemical Society: Washington, DC, 1989; pp 11–27.
(38) (a) Van Santen, R. A.; Keijsper, J. J.; Ooms, G.; Kortbeek, A. G. T. G. *Stud. Surf. Sci. Catal.* **1986**, *28*, 169–175. (b) Groenen, E. J. J.; Kortbeek, A. G. T. G.; Mackay, M.; Sudmeijer, O. *Zeolites* **1986**, *6*, 403–411. (c) Van den Berg, J. P.; De Jong-Versloot, P. C.; Keijsper, J. J.; Post, M. F. M. In *Studies in Surface Science & Catalysis*; Grobet, P. J., Mortier, W. J., Vansant, E. F., Schuiz-Ekloff, G., Eds.; Elsevier Science: 1983; Vol. 37, pp 85–95. (d) Keijsper, J. J.; Post, M. F. M. In *ACS Symposium Series 398, Zeolite Synthesis*; Occelli, M. L., Robson, H. E., Eds.; American Chemical Society: Washington, DC, 1989; pp 28–47.
(39) Tiddy, G. J. T. *Phys. Rep.* **1980**, *57*, 1–46.
(40) Speght, P. P. A.; Skoulios, A. E.; Luzzati, V. *Acta Crystallogr.* **1961**, *14*, 866–872.
(41) Komarov, V. S.; Kuznetsova, T. F. *Vestsi Akad. Navuk BSSR* **1978**, *2*, 22–27.
(42) (a) Freude, D.; Hunger, M.; Pfeifer, H.; Schwieger, W. *Chem. Phys. Lett.* **1986**, *128*, 62–66. (b) Chester, A. W.; Chu, Y. F.; Dessau, R. M.; Kerr, G. T.; Kresge, C. T. *J. Chem. Soc., Chem. Commun.* **1985**, 289–290. (c) Hunger, M.; Freude, D.; Frohlich, T.; Pfeifer, H.; Schwieger, W. *Zeolites* **1987**, *7*, 108–110. (d) Engelhardt, G.; Jerschkewitz, H.-G.; Lohse, U.; Sarv, P.; Samoson, A.; Lippmaa, E. *Zeolites* **1987**, *7*, 289–292. (e) Brunner, E.; Ernst, H.; Freude, D.; Hunger, M.; Pfeifer, H. In *Studies in Surface Science & Catalysis*; Grobet, P. J., Mortier, W. J., Vansant, E. F., Schuiz-Ekloff, G., Eds.; Elsevier Science: 1988; Vol. 37, pp 155–165. (f) Hunger, M.; Freude, D.; Pfeifer, H.; Schwieger, W. *Chem. Phys. Lett.* **1990**, *167*, 21–24.

Figure 12. Transmission electron micrographs (a, b, and d) and scanning electron micrograph (c) of MCM-41.

Surfactant/Silicon Ratio Studies—Isolation of Other Phases. In addition to the isolation of the hexagonal MCM-41 class, other materials with different geometries were synthesized. Some of these were prepared by varying the surfactant to silicon mole ratio. At a $C_{16}H_{33}(CH_3)_3N^+$/Si ratio of less than 1, the predominant product appears to be the hexagonal phase, MCM-41. As the $C_{16}H_{33}(CH_3)_3N^+$/Si ratio increases beyond 1, a cubic phase can be produced. The diffraction data of the cubic phase are consistent with space group *Ia3d* (see Figure 13a). As the $C_{16}H_{33}$-$(CH_3)_3N^+$/Si ratio increases further another material is formed which exhibited fairly well defined XRD patterns in the as-synthesized form but, upon calcination, lost all XRD pattern definition. The XRD patterns of these as-synthesized products characteristically display multiple peaks that are higher orders of the first peak, as illustrated in Figure 13b, suggesting a lamellar type material. At $C_{16}H_{33}(CH_3)_3N^+$/Si ratios approaching 2, a non M41S phase, the organic octamer, identified from its Si-NMR, is formed $[(C_{16}H_{33}(CH_3)_3N)SiO_{2.5}]_8$.[33] The cubic phase and other less well defined phases that are observed indicate the extensive M41S family of mesoporous molecular sieves.

Discussion

The M41S materials described herein are the initial members of a new family of mesoporous molecular sieves. They exhibit a periodic pore system. The pore size of at least one member, MCM-41, can be varied from ~18 to over 100 Å in a continuous, controllable manner.

The microscopy and diffraction results presented for MCM-41 are strikingly similar to those obtained[34] from surfactant/water liquid crystal or micellar phases. This leads us to propose a "liquid crystal templating" (LCT) mechanism for the formation of the

M41S materials.[14] The LCT mechanism exploits the continuous solvent (water) region to create inorganic walls between the surfactant liquid crystal structure. It may be that encapsulation occurs because anionic inorganic species enter the solvent region to balance the cationic hydrophilic surfaces of the micelles. Alternatively, perhaps it is the introduction of the inorganic species themselves that mediates the liquid crystal ordering. M41S formation differs from that of normal zeolite crystallization principally in its timing. One model for zeolite crystallization proposes silicate condensation about a template molecule or ion. The initial ordered species may be an aggregate of water molecules[35] or silicate moieties.[36] Subsequent growth may arise because of nucleation by this initial structure[37] or assembly of a number of such substructures[38] but growth is the consequence of the initial silicate organization. In the LCT mechanism, we propose that silicate *condensation* is not the dominant factor in the formation of the structure. We suggest that the structure is defined by the organization of the surfactant molecules into micellar liquid crystals which serve as templates for the formation of the MCM-41 structure. For this reason, the types of materials which may be formed are certainly not limited to silicates, nor must these materials necessarily have regularly repeating secondary building units (SBUs) in the pore walls in order to form the regularly repeating porous networks observed.

We do not mean to imply, however, that the aqueous silicate species are irrelevant to the formation of M41S. The liquid crystal structures which form in surfactant solutions are highly sensitive to solution conditions. Ionic strength, counterion polarizability, surfactant concentration, counterion charge, temperature, and the addition of co-surfactants or additives like alcohols or hydrocarbons
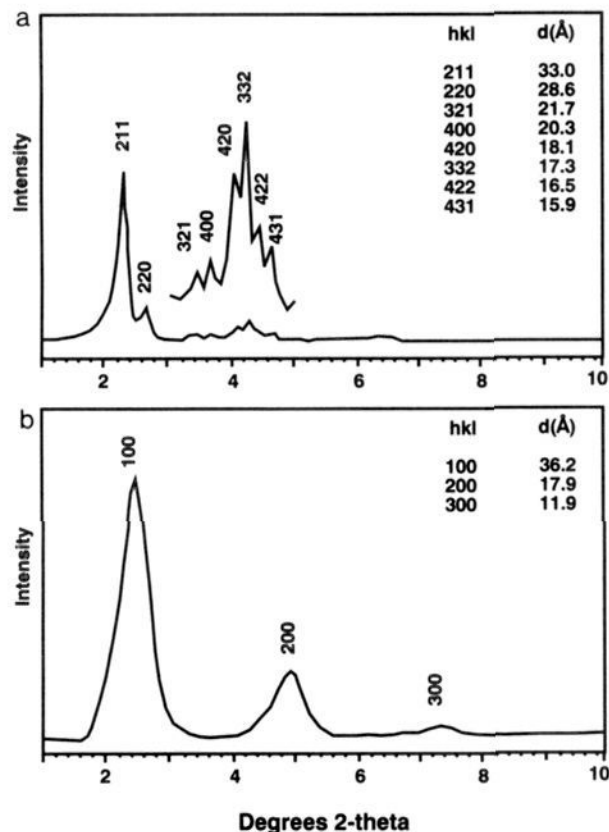
10842 *J. Am. Chem. Soc., Vol. 114, No. 27, 1992*

Beck et al.

a

hkl	d(Å)
211	33.0
220	28.6
321	21.7
400	20.3
420	18.1
332	17.3
422	16.5
431	15.9

b

hkl	d(Å)
100	36.2
200	17.9
300	11.9

Degrees 2-theta

Figure 13. Powder X-ray diffraction patterns of (a) calcined cubic material and (b) the as-synthesized unstable lamellar material.

are all factors known to shift surfactant solutions from micellar to any of a number of liquid crystalline phases. "Silica" itself is a complex system of molecular and polymeric anionic species whose composition and concentration can be expected to exercise control over the liquid crystalline phase which forms and is subsequently trapped by silicate *condensation*. Therefore, we propose two possible pathways. One in which the liquid crystal phase is intact before the silicate species are added and two in which the addition of the silicate results in the ordering of the subsequent silicate encased surfactant micelles. However, in either case, the resultant composition (surfactant/silicate) produces an inorganic material that mimics known liquid crystal phases.

The liquid crystal mechanism of M41S formation suggests that the as-synthesized materials will have the micellar structures included intact. As-synthesized MCM-41 materials contain surfactant molecules most likely still arranged in a micellar array. In fact, MCM-41 materials do form with the pores containing surfactant and C-NMR indicates this phase is quite similar to liquid crystalline phases.

The experimental data for the formation of the hexagonal MCM-41 are consistent with the aggregation of $C_nH_{2n+1}(CH_3)_3N^+$

surfactant micelles into rods. These structures are known to exist in a hexagonal arrangement in solution.[39] Inorganic silicate present in the reaction mixtures could then form around these arrays to produce an inorganic structure, reflecting the hexagonal micellar array (pathway 1 of Figure 14). Figure 14 also illustrates another possible mechanistic pathway in which the silicate influences the formation of this liquid crystal phase (reaction pathway 2). In either case, the resultant silicate encased hexagonal structure produces the desired MCM-41 material. The carbon chain length of the surfactant plays a role in determining the dimensions of $C_nH_{2n+1}(CH_3)_3N^+$ micelles[34] and, as we have shown, in the dimensions of the pores of MCM-41.

Liquid crystal phases are capable of solubilization of organic molecules within their hydrophobic interiors.[34] The hexagonal phase of ethylbenzene/sodium myristate/water containing no silicate, for example, can be swollen in proportion to the amount of solubilized ethylbenzene.[40] The effect of adding solubilizates to surfactant solutions to increase the porosity of amorphous alumina adsorbents has been reported.[41] Our aluminosilicate containing hexagonal systems, MCM-41, also show pore diameters which increase in proportion to the amount of mesitylene added to the synthesis mixture, but only if the mesitylene is added at an early stage of the gelation process. This strongly suggests that the liquid crystal structure is the defining structure.

The formation of the cubic phase by changing the surfactant to silicate ratio also supports the liquid crystal templating mechanism, since this variation in reactant composition changes both the surfactant concentration and the ionic strength, either of which can induce liquid crystal phase changes.[34] The existence of a lamellar phase would also be consistent with liquid crystal phase transitions.

The presence and distribution of silanol groups in MCM-41 materials shown by MAS Si-NMR and derivatization is also consistent with the proposed mechanism. Silanols are present in amorphous silicas at a level which depends on calcination temperature.[24] Silanols are often present in zeolites either as random defects or charge balancing siloxy groups.[42] In siliceous MCM-41 materials, silanols can be expected to be present as charge balancing groups associated with the quaternary ammonium ions with a spacing which, at least roughly, approximates the spacing of the surfactant molecules in the micelles.

Conclusion

M41S represents a new family of mesoporous molecular sieve materials. MCM-41, the hexagonal phase, is characterized as having a uniform and controllable pore size from ~15 to greater than 100 Å, high surface area, and high hydrocarbon sorption capacity. These molecular sieves are formed by a mechanism in which surfactant liquid crystal phases are believed to serve as templates. In support of this templating mechanism, the structure and pore dimensions of MCM-41 materials are intimately linked to the properties of the surfactant, such as surfactant chain length, solution chemistry and micellar solubilization of trimethylbenzene. The existence of other phases, including a cubic phase, supports this LCT mechanism and indicates that M41S is an extensive family of materials.
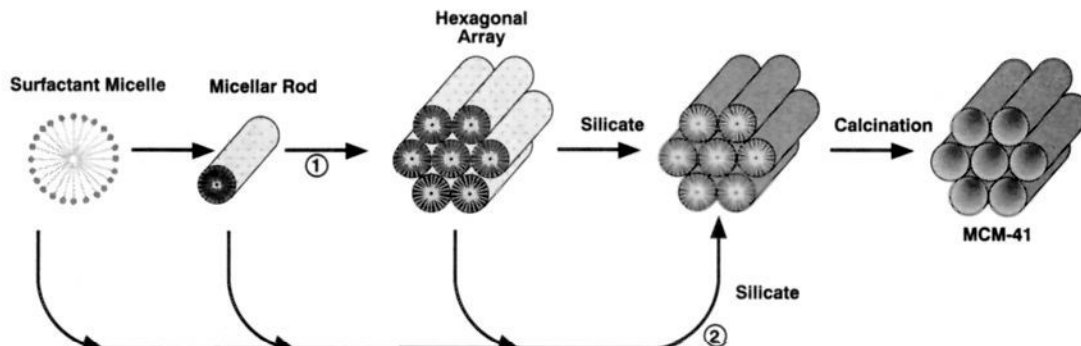
Figure 14. Possible mechanistic pathways for the formation of MCM-41: (1) liquid crystal phase initiated and (2) silicate anion initiated.

Synthesis and Comparative Reactivity and Electronic Structural Features of $[MFe_3S_4]^{z+}$ Cubane-Type Clusters (M = Fe, Co, Ni)

Jian Zhou,[†] Michael J. Scott,[†] Zhengguo Hu,[§] Gang Peng,[†] E. Münck,[*,§] and R. H. Holm[*,†]

Contribution from the Departments of Chemistry, Harvard University, Cambridge, Massachusetts 02138, and Carnegie Mellon University, Pittsburgh, Pennsylvania 15213. Received July 2, 1992. Revised Manuscript Received August 27, 1992

Abstract: The heterometal cubane-type clusters $[CoFe_3S_4(Smes)_4]^{2-}$ (**7**, 80%) and $[NiFe_3S_4(PPh_3)(Smes)_3]^{2-}$ (**12**, 57–71%) have been prepared in good yield as Et_4N^+ salts by reductive rearrangement reactions of the linear cluster $[Fe_3S_4(Smes)_4]^{3-}$ (**4**, Smes = mesitylthiolate(1–)) with Co(I) and Ni(0) reactants, respectively. $(Et_4N)_2[7]$ crystallizes in orthorhombic space group *Pbcn* with $a = 20.673$ (3) Å, $b = 16.600$ (3) Å, $c = 17.259$ (2) Å, and $Z = 4$. $(Et_4N)_2[NiFe_3S_4(PPh_3)(Smes)_3]\cdot2MeCN$ was obtained in triclinic space group $P\bar{1}$ with $a = 13.138$ (3) Å, $b = 15.461$ (4) Å, $c = 19.622$ (4) Å, $\alpha = 107.12$ (2)°, $\beta = 94.54$ (2)°, $\gamma = 108.47$ (2)°, and $Z = 2$. The crystal structures confirm the cubane-type structures and tetrahedral coordination at the M = Fe, Co, and Ni subsites of the $[MFe_3S_4]^{z+}$ cores. In **7**, the Co and Fe subsites are disordered and in **12** the phosphine ligand is bound to the Ni subsite. The clusters $[NiFe_3S_4(Smes)_4]^{3-}$ (**10**) and $[Fe_4S_4(Smes)_4]^{2-}$ (**6**) were obtained as an ca. 1:1 mixture by the reaction of $Ni(AsPh_3)_4$ and **4**. Potential and actual synthetic routes to $[MFe_3S_4]^{z+}$ clusters are outlined. The species **6**, **7**, **10** form a comparative set with equivalent structures and identical terminal ligands. These species and **12** are best distinguished by their ^1H NMR spectra which manifest contact-shifted resonances that are oppositely signed for substituents at the Fe and M = Co/Ni subsites. In **7**, the Fe subsites appear to be more reactive to ligand substitution by thiol than is the Co subsite; both subsites are substituted in the ligand redistribution system **5**/**7**. The three-member electron transfer series $[CoFe_3S_4]^{3+/2+/1+}$ and $[NiFe_3S_4]^{2+/1+/0}$ have been established. For the reversible couples $[MFe_3S_4(Smes)_4]^{2-/3-}$ the order of potentials is M = Fe < Co (0.18 V) < Ni (0.30 V), with the indicated potential differences vs M = Fe. Mössbauer spectroscopy reveals that **7** and the protein-bound $[CoFe_3S_4]^{2+}$ cluster of *D. gigas* ferredoxin II have equivalent electronic structures at 4.2 K. As judged by isomer shifts at 1.5 K, the $[NiFe_3S_4]^{1+}$ core of polycrystalline **12** contains three equivalent iron sites. However, the 4.2 K Mössbauer spectra obtained in strong applied magnetic fields show clearly that the three sites are magnetically distinct. Interestingly, the room temperature solution ^1H NMR data of **7** and **12** indicate equivalent sites. Isomer shifts imply the fragment formulations Co^{2+} $(S = ^3/_2) + [Fe_3S_4]^0$ $(S = 2)$ and Ni^{2+} $(S = 1) + [Fe_3S_4]^{1-}$ $(S = ^5/_2)$, with antiparallel spin coupling affording the observed $S = ^1/_2$ and $^3/_2$ ground states, respectively. Comparison of the isomer shifts of the $[NiFe_3S_4]^{1+}$ core with those of other $[MFe_3S_4]^{1+}$ cubanes (M = Fe, Zn, Cd) suggests a shifted electron density from the $[Fe_3S_4]^{1-}$ fragment to the nickel site. The close correspondence of Mössbauer and EPR parameters of synthetic clusters (**7**, **12**) with those of protein $[CoFe_3S_4]^{2+}$ and $[NiFe_3S_4]^{1+}$ clusters indicates that the latter contain the tightly bound cubane-type structures established by X-ray diffraction for the synthetic species.

Introduction

The protein-bound cluster $Fe_3S_4(S\cdot Cys)_3$ is now recognized, on the basis of its characteristic EPR, Mössbauer, and MCD spectroscopic properties, to occur in a relatively large number of iron–sulfur proteins and enzymes.[1,2] Its cuboidal structure **1**, illustrated in Table I, has been demonstrated by X-ray analysis of three proteins.[3–5] While the biological function (if any) of this cluster remains obscure, it possesses at least two properties of current significance in the field of metal clusters in biology. One of these involves reactivity and the second electronic structure.

Trinuclear cluster **1**, when in the $[Fe_3S_4]^{0,1-}$ core oxidation states, has a binding affinity for certain divalent metal ions that affords the cubane-type clusters **2**.[6–15] The situation is summarized in Table I, from which it is evident that ferredoxin proteins (note abbreviations) may be reconstituted in reaction 1 to a homometallic (Fe_4S_4) or to heterometallic (MFe_3S_4) species. In the remaining known oxidation state of **1**, $[Fe_3S_4]^{1+}$, the electrophilic

demands of three Fe^{3+} sites render the sulfur atoms insufficiently basic to bind divalent ions of the first transition series. Binding

(1) (a) Beinert, H.; Thomson, A. J. *Arch. Biochem. Biophys.* **1983**, *222*, 333. (b) Beinert, H.; Kennedy, M. C. *Eur. J. Biochem.* **1989**, *186*, 5. (c) Beinert, H. *FASEB J.* **1990**, *4*, 2483. (d) Cammack, R. *Adv. Inorg. Chem.* **1992**, *38*, 281.

(2) Holm, R. H. *Adv. Inorg. Chem.* **1992**, *38*, 1.

(3) Robbins, A. H.; Stout, C. D. *Proc. Natl. Acad. Sci. U.S.A.* **1989**, *86*, 3639; *Proteins* **1989**, *5*, 289.

(4) Stout, C. D. *J. Biol. Chem.* **1988**, *263*, 9256; *J. Mol. Biol.* **1989**, *205*, 545.

(5) (a) Kissinger, C. R.; Adman, E. T.; Sieker, L. C.; Jensen, L. H. *J. Am. Chem. Soc.* **1988**, *110*, 8721. (b) Kissinger, C. R.; Sieker, L. C.; Adman, E. T.; Jensen, L. H. *J. Mol. Biol.* **1991**, *219*, 693.

(6) (a) Kent, T. A.; Dreyer, J.-L.; Kennedy, M. C.; Huynh, B. H.; Emptage, M. H.; Münck, E. *Proc. Natl. Acad. Sci. U.S.A.* **1982**, *79*, 1096. (b) Beinert, H.; Emptage, M. H.; Dreyer, J.-L.; Scott, R. A.; Hahn, J. E.; Hodgson, K. O.; Thomson, A. J. *Proc. Natl. Acad. Sci. U.S.A.* **1983**, *80*, 393. (c) Kennedy, M. C.; Emptage, M. H.; Dreyer, J.-L.; Beinert, H. *J. Biol. Chem.* **1983**, *258*, 11098. (d) Emptage, M. H.; Dreyer, J.-L.; Kennedy, M. C.; Beinert, H. *J. Biol. Chem.* **1983**, *258*, 11106. (e) Kent, T. A.; Emptage, M. H.; Merkle, H.; Kennedy, M. C.; Beinert, H.; Münck, E. *J. Biol. Chem.* **1985**, *260*, 6871.

† Harvard University.
§ Carnegie Mellon University.